Total scattering and reverse Monte Carlo study of the 105 K displacive phase transition in strontium titanate

Qun Hui[1]**, Matthew G Tucker**[1]**, Martin T Dove**[1]**, Stephen A Wells**[1] **and David A Keen**[2,3]

[1] Department of Earth Sciences, University of Cambridge, Downing Street,
Cambridge CB2 3EQ, UK
[2] Physics Department, Oxford University, Clarendon Laboratory, Parks Road,
Oxford OX1 3PU, UK
[3] ISIS Facility, Rutherford Appleton Laboratory, Chilton, Didcot, Oxon OX11 0QX, UK

Abstract

We report a study of the displacive phase transition in $SrTiO_3$ using neutron total scattering with analysis by the reverse Monte Carlo method. The resultant configurations have been analysed in terms of bond distance and bond angle distribution functions, and using recently developed methods based on geometric algebra (GA). The resultant picture is that the short-range order in $SrTiO_3$ closely follows the long-range order, with very little disorder in the high-temperature phase. This result is in contrast to similar work carried out on the displacive phase transition in quartz (Tucker *et al* 2000 *J. Phys.: Condens. Matter.* **12** L723–30). The differences between these two systems arises from the fact that there are many more Rigid Unit Modes in quartz, a point that is quantified by the GA analysis.

(Some figures in this article are in colour only in the electronic version)

1. Introduction

The displacive phase transition at 105 K in $SrTiO_3$ [1] has become one of the archetype examples of a displacive phase transition, alongside systems such as quartz and the ferroelectric perovskites. The initial interest in this phase transition arose from the facts that the displacive phase transition is second-order (continuous), with an easily accessible transition temperature. The soft modes were measured by both Raman scattering [2] and neutron scattering [3, 4], giving clean results that enabled $SrTiO_3$ to play the role of a nice example of the soft-mode picture of the phase transition. Moreover, the fact that the phase transition is continuous meant that it was a good system for the study of critical phenomena, and indeed several early sets of results showed departures of several properties from classical mean-field behaviour (see [5]). The situation was muddied somewhat through subsequent studies of the dynamical

properties close to the transition temperature, with features such as the central peak and the incomplete softening of the soft mode that are inconsistent with the traditional soft mode model (summarized in [1] and [5]). These studies led to the need to consider the role of defects and surfaces on the behaviour of displacive phase transitions [6, 7]. Recently it has been suggested that the 105 K phase transition in $SrTiO_3$ can be fully described by classical mean-field behaviour provided that the Landau free energy function is extended to terms of higher order than normal [8–10]. In addition to the structural instability at 105 K, there is an incipient ferroelectric phase transition at 0 K. In fact the ferroelectric soft mode would classically become unstable at around 30 K, but the quantum fluctuations inhibit the ferroelectric phase transition. There has been subsequent work on the quantum paraelectric state of $SrTiO_3$ [11–16], but we are not concerned with this in the present study. Indeed, previous neutron diffraction work [17] has suggested that these effects are not easily seen in diffraction measurements. To conclude this brief review, we also note that there has also been work on the domain structure associated with the phase transition [18, 19].

It is quite possible that the phase transition in $SrTiO_3$, together with that in quartz, is one of the best studied of all displacive phase transitions. Because of this, it is interesting to apply new techniques to this system as they become available, partly to provide a useful benchmark, and partly to see if the new technique can provide new insights. In this paper we report a study of the phase transition in $SrTiO_3$ using neutron total scattering, with the results being analysed using the reverse Monte Carlo method [20–23]. Although this is not a new technique *per se*, the new GEM diffractometer at the ISIS spallation source [24] opens up this experimental technique for the study of the types of subtle structural changes that accompany displacive phase transitions. Moreover, coupled with the development of GEM has been a lot of development work on the application of the RMC method for the study of crystalline materials, in particularly to take explicit account of the information on long-range order contained within the Bragg peaks to augment the information on short-range order contained in the total scattering [22, 23]. Recent examples of the use of RMC for the study of displacive phase transitions include our work on quartz [25, 26] and cristobalite [27]. $SrTiO_3$ is more challenging for two reasons. *First*, the phase transition in $SrTiO_3$ involves much smaller atomic displacements, and *second*, there are three atomic species and hence six distinct partial pair distribution functions (ppdfs) in $SrTiO_3$, compared to two atomic species and three ppdfs in quartz and cristobalite.

In this paper we briefly review the structural details of the phase transition in $SrTiO_3$ and the details of the method. We then report some of the information that is readily extracted from the RMC analysis (including bond angle distribution functions). Finally we apply new analysis methods developed using geometric algebra to provide new information about the nature of the dynamic disorder associated with the phase transition and to determine the fraction of the dynamical disorder that can be associated with TiO_6 rotational phonon modes.

2. 105 K displacive phase transition in $SrTiO_3$

The average crystal structures of the two phases of $SrTiO_3$ are shown in figure 1. The high-temperature phase is the standard cubic perovskite structure, with space group $Pm3m$. The low-temperature phase has a tetragonal structure, with space group $I4/mcm$. The lattice vectors of the two phases are related by the following transformation matrix:

$$\begin{pmatrix} \mathbf{a} \\ \mathbf{b} \\ \mathbf{c} \end{pmatrix}_{I4/mcm} = \begin{pmatrix} 1 & -1 & 0 \\ 1 & 1 & 0 \\ 0 & 0 & 2 \end{pmatrix} \times \begin{pmatrix} \mathbf{a} \\ \mathbf{b} \\ \mathbf{c} \end{pmatrix}_{Pm3m}. \tag{1}$$
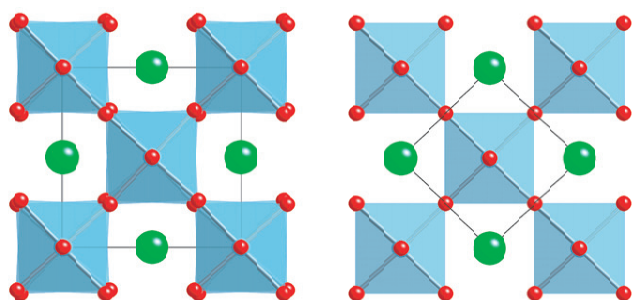
Figure 1. Crystal structures of the low-temperature (left) and high-temperature (right) phases of SrTiO₃, highlighting the TiO₆ octahedra and showing the Sr cations as spheres.

One way to view the structural changes accompanying the phase transition is to consider the TiO₆ octahedron to move as a nearly-rigid entity. In this representation, the structure of SrTiO₃ consists of corner-sharing octahedra. The phase transition can then be said to occur as the result of counter-rotations of neighbouring octahedra about the tetragonal four-fold axis, with maximum rotation of just ∼2°. This picture may be faulted because it is known that the octahedra are slightly distorted in the low-temperature phase, and because in the ferroelectric phase transitions in the titanate perovskites the Ti cation moves off the centre of the TiO₆ polyhedron. However, there is a lot of merit in the nearly-rigid picture when considering the dynamics. If the forces operating within the TiO₆ octahedra are stronger than other forces in the crystal, including the bending forces at the Ti–O–Ti linkage in the x–y plane, and torsional forces in the z-direction, it can be shown that the phonon spectra contain a potential soft mode along the edges of the Brillouin zone, i.e. for wavevectors of the form $\langle \frac{1}{2}, \frac{1}{2}, \xi \rangle$ [29]. This is supported by inelastic neutron scattering measurements [30].

The polyhedral viewpoint has been particularly well exploited in studies of silica-based materials such as quartz. In these cases the fundamental polyhedra are SiO₄ or AlO₄ tetrahedra, linked together at the corners just as in the perovskite structure. This approach, encompassed within the 'Rigid Unit Mode' (RUM) model [29], has been used to understand the origin of displacive phase transitions in silicates [25, 26, 31, 32], and to understand the nature of high-temperature phases [27, 33]. There is a fundamental difference between many silicates and perovskites in the RUM approach. We have noted that the rotational phonon instabilities (RUMs) for the perovskite structure are restricted to lines in reciprocal space (the edges of the Brillouin zone). However, in silicates we typically find that there are whole planes of RUMs. Thus we expect that silicate structures will be much more flexible than perovskite structures. We are able to address this comparison quantitatively in this paper.

3. Methods

3.1. Experimental method and data analysis

The measurements of the neutron total scattering function were performed on a finely ground powder sample of strontium titanate using the GEM diffractometer at the ISIS pulsed spallation neutron source [24]. GEM is a time-of-flight diffractometer with banks of detectors that cover most of the available scattering angles. Diffraction patterns can be collected to high values of the scattering vector Q, of order 50 Å⁻¹. This ensures that we obtain good real-space resolution ($\Delta r \simeq 2\pi/Q_{max}$; using $Q_{max} = 50$ Å⁻¹ implies $\Delta r \simeq 0.13$ Å). The sample was obtained commercially (Aldrich Chemicals). The powder had a grain size of less than 5 μm and was 99% pure. The sample used in the experiment was contained in a cylindrical vanadium can of 1.1 cm diameter and 4 cm height. This was mounted within a closed-cycle
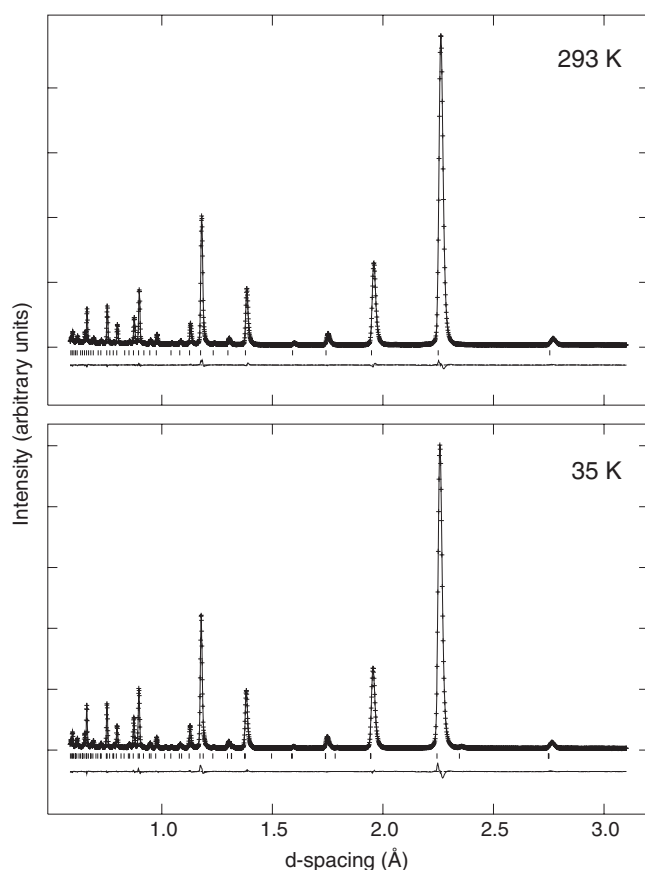
Figure 2. Diffraction patterns from SrTiO$_3$ obtained at two temperatures on the high-angle bank of detectors on GEM, showing data (crosses), fitted patterns (line), positions of expected reflections (tick marks) and differences (data-fit) (lower traces).

helium refrigerator (CCR). Long measurements for subsequent RMC analysis were obtained at temperatures of 5, 50, 75, 105, 150, 200, 250 and 293 K. Shorter measurements for Rietveld analysis only were obtained at 20, 30, 40, 60, 70, 85, 95, 115, 125, 135, 145, 160, 170, 180, 190, 210, 220, 230, 240, 260, 270, and 280 K.

Standard methods were used to correct the data for subsequent analysis as total scattering data. These are described elsewhere [23].

3.2. Rietveld analysis

Rietveld refinement was carried out on all data sets using the GSAS code [34, 35]. For temperatures below 105 K the initial structure model was the standard tetragonal $I4/mcm$ model with one independent variable atomic fractional coordinate, and for higher temperatures we used the ideal $Pm3m$ structure model. In both temperature ranges we used the output from one temperature data set as the input for the next temperature in the sequence. We refined isotropic temperature factors for the Sr and Ti atoms, and anisotropic temperature factors for the O atoms, in both phases. Lattice parameters were also refined in both phases. Because the splitting of Bragg peaks in the low-temperature phase is slight, we fixed the values of the peak profile parameters for the data in this phase at the values refined for the data in the high-temperature phase. Representative fitted diffraction patterns are shown in figure 2.
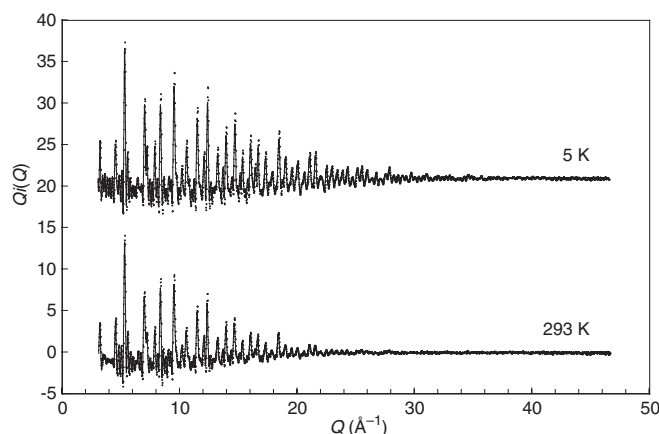
Figure 3. Representative $Qi(Q)$ data for SrTiO$_3$ for two temperatures, obtained on the $2\theta \simeq 90°$ bank of detectors on GEM. The points are the experimental data, and the lines show the fit obtained using RMC.
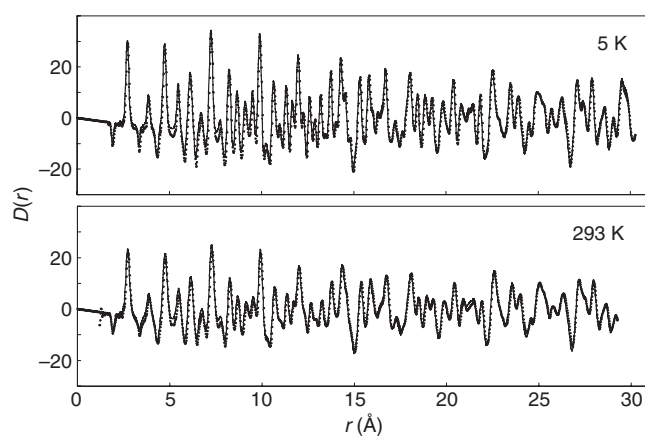

Figure 4. $D(r)$ data obtained by Fourier transform of the $Qi(Q)$ data as described in the text. The points show the experimental data, and the lines show the fit obtained using RMC. Note that Ti has a negative neutron scattering length, leading to some peaks having negative weight.

3.3. RMC analysis

The method used for the RMC analysis has been described in detail elsewhere [22, 23]. Of note in our case is the fact that we explicitly use the Bragg diffraction data in addition to the total scattering data. Although the total scattering data include the Bragg peaks, through handling the Bragg scattering separately it is possible to separate the information contained in the long-range order contained in the Bragg peaks from the shorter-range order contained within the total scattering data in the RMC analysis. Moreover, through the assignment of the Miller indices of the Bragg peaks, in some senses this adds a three-dimensional component to the RMC method. We used data-based constraints to prevent atoms moving away from their equilibrium positions (soft constraints on the Ti–O distance and on the O–Ti–O angles), as described in [22] and [23]. We did note the tendency for our RMC configurations to generate internal interfaces, which we associated with the effects of small errors in the data, and which could be overcome by careful use of soft constraints. Representative fitted normalized total structure factors, $Qi(Q)$, and total pair distribution functions, $D(r)$ data, as defined in [36], are shown in figures 3 and 4 respectively. A representative RMC configuration obtained from the data of 293 K is shown in figure 5.
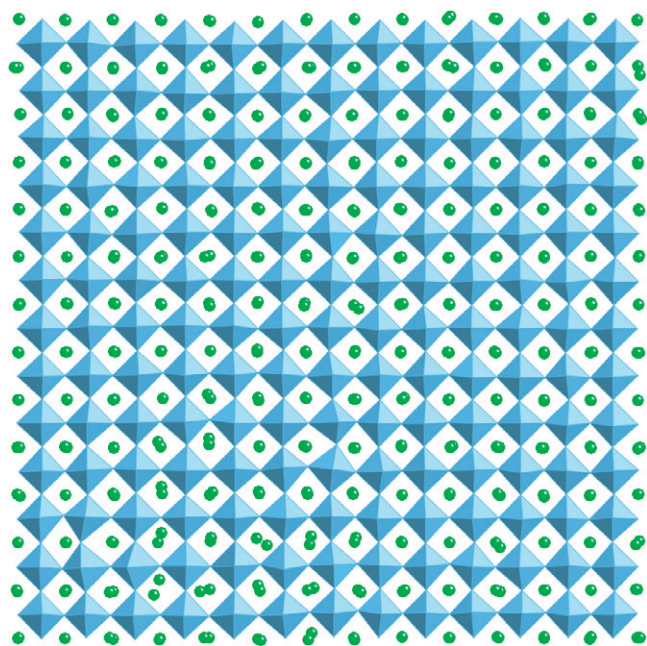
Figure 5. Single layer of TiO_6 octahedra extracted from an RMC configuration obtained from analysis of the 293 K data. The TiO_6 octahedra are shown as solid objects. The Sr atoms in the layers above and below the Ti layer are shown as spheres.
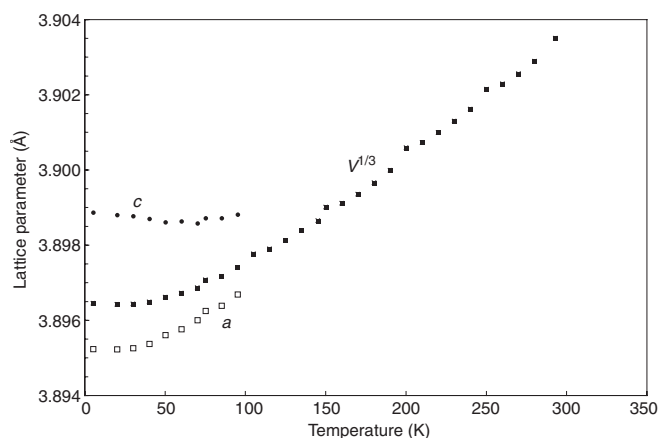

Figure 6. Temperature dependence of the lattice parameters obtained from our Rietveld refinements. The data for a and c in the low-temperature phase have been scaled by factors of $\sqrt{2}$ and 2 respectively to match the data in the high-temperature phase. $V^{1/3}$ is the cube root of the volume of one formula unit and is equivalent to the lattice parameter in the high-temperature cubic phase.

4. Results

4.1. Results from Rietveld refinement: long-range structural order

Crystallographic results from Rietveld analysis are given in table 1. Cell parameters at different temperatures are plotted in figure 6, together with the temperature dependence of the cube root of the reduced unit cell volume. The finite resolution of the diffraction data mean that the lattice parameters for temperatures just below the transition temperature are able to show a greater splitting than reality (when comparing $\sqrt{2}a$ with $c/2$), as is seen in figure 6.

Table 1. Summary of the Rietveld refined structural parameters of SrTiO₃. Below 105 K the space group is $I4/mcm$; above this the space group is $Pm3m$. In the tetragonal phase, O atoms sit at $(0, 0, \frac{1}{4})$ and $(\frac{1}{4} - u, \frac{3}{4} - u, 0)$. Errors are typically 1, 3, and 8 in the last decimal place for a, c and u, respectively.

Temperature (K)	a (Å)	c (Å)	u
5	5.508 7	7.7978	0.008 57
20	5.508 7	7.7976	0.008 59
30	5.508 7	7.7976	0.008 46
40	5.508 9	7.7974	0.008 18
50	5.509 2	7.7972	0.007 97
60	5.509 5	7.7973	0.007 62
70	5.509 8	7.7972	0.007 25
75	5.510 1	7.7975	0.006 80
85	5.510 3	7.7975	0.006 37
95	5.510 8	7.7976	0.005 84
105	3.897 77		
115	3.897 90		
125	3.898 13		
135	3.898 39		
145	3.898 66		
150	3.899 01		
160	3.899 12		
170	3.899 36		
180	3.899 66		
190	3.899 99		
200	3.900 60		
210	3.900 73		
220	3.901 00		
230	3.901 30		
240	3.901 62		
250	3.902 15		
260	3.902 29		
270	3.902 57		
280	3.902 89		
293	3.903 51		

The square of the TiO₆ [001] rotation angle is plotted as a function of temperature in figure 7. The results in figure 7 are consistent with the summary of earlier data presented by Kiat and Roisnel [17], as shown in figure 7. Moreover, apart from the two data points close to the phase transition, the Rietveld data compare well to the fitted temperature dependence of the square of the rotation angle obtained by Hayward and Salje [8]. It is likely that the slight exaggeration of the value of the rotation angle obtained from our Rietveld analysis arises from small errors in the data, including errors in the lattice parameters (discussed above).

The Ti–O and Sr–O distances from the average positions obtained by the Rietveld structure solution are plotted in figure 8, where (see below) we make an important comparison with the results from the RMC analysis. We reiterate that the results from the Rietveld refinement give information about the long-range order and average positions, and later we will compare these results with analysis of the RMC configurations, which give information about instantaneous interatomic distances.

4.2. RMC analysis

4.2.1. Nearest-neighbour interatomic distances. The Ti–O and Sr–O first-neighbour partial pair distribution functions are shown in figure 9. We have separated the distances for contacts
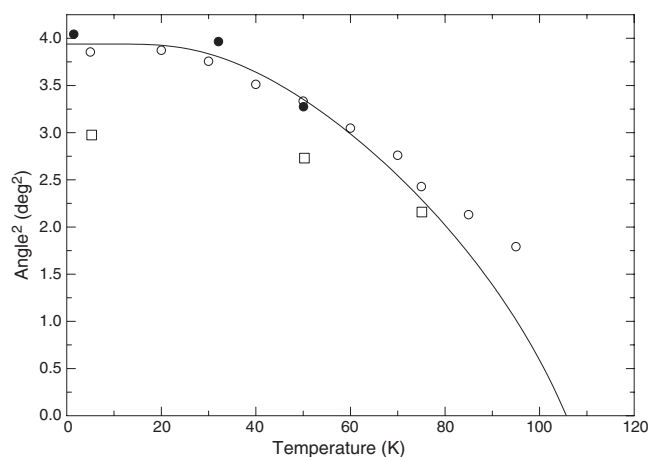
Figure 7. Square of the TiO_6 rotation angle obtained from the present Rietveld analysis (open circles), the RMC analysis (open squares), and from the data of Kiat and Roisnel [17] (filled circles). The curve is from the Landau theory of Hayward and Salje [8].
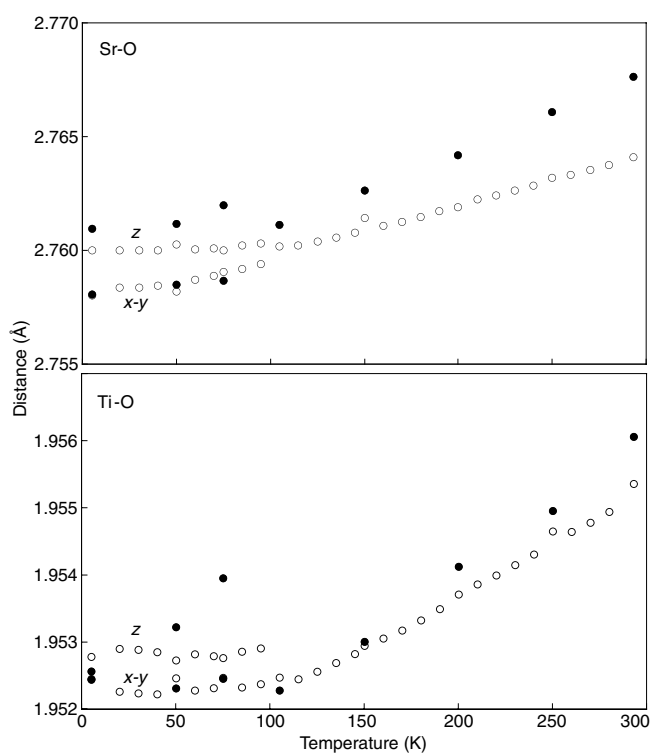

Figure 8. Sr–O and Ti–O distances obtained by Rietveld analysis (open circles) and RMC (filled circles), differentiating between bonds lying parallel (marked as 'z') and normal (marked as 'x–y') to the [001] direction. The Rietveld results in both cases have had 0.035 Å added to their values to bring the RMC and Rietveld data onto the same plots.

along the [001] direction from the contacts in the (001) plane. The clear impression from these plots is that changes in the mean positions are smaller than the widths of the peaks in the distribution functions. It should also be noted that the widths, of 0.16 and 0.24 Å respectively, are only slightly larger than the real-space resolution (0.13 Å; see above). The mean positions are plotted in figure 8 for comparison with the Rietveld results. The RMC mean distances in both cases are consistently slightly higher than the Rietveld distances, by around 0.0035 Å, which is much smaller than the real-space resolution and smaller than the histogram bin size used in the RMC (0.02 Å). Thus we believe that this small difference is probably due to rounding
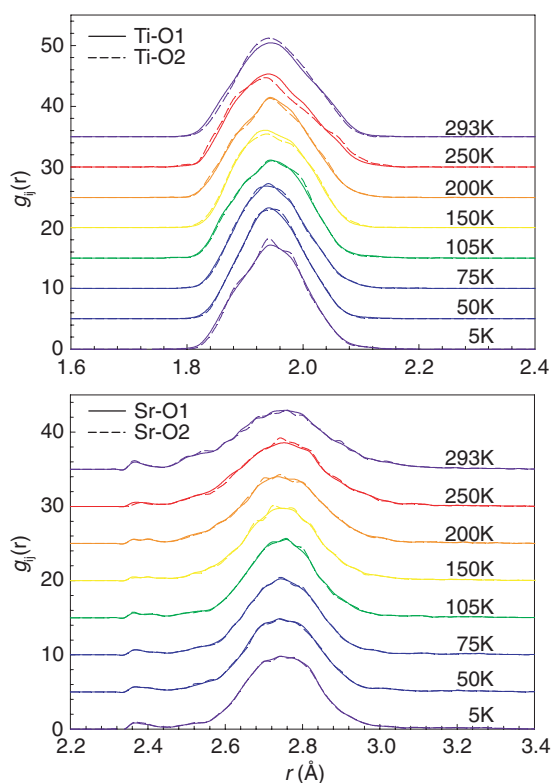
Figure 9. Ti–O and Sr–O nearest-neighbour peaks in the partial pair distribution functions. Note that the small peak in the Sr–O pair distribution function is an artefact in the simulation.

errors and is unlikely to be a significant artefact. We have shifted the Rietveld results for both distances by this small amount in figure 8 in order to aid comparison between the trends in the Rietveld and RMC data. We note that the trends in the Rietveld and RMC analyses are similar except in one respect (see below). We particularly note that the same small differences between the interatomic distances in the [001] direction and in the (001) plane are seen in the two types of analysis, although from figure 9 it is clear that these differences are not significant.

The main significant difference between the trends in the RMC and Rietveld distances in figure 8 concerns the slopes of the data in the high-temperature phase. For both types of distances, the coefficient of thermal expansion of the interatomic distances is slightly larger in the RMC data than in the Rietveld results. The data for the high-temperature phase shown in these two figures have been fitted by straight lines to yield values for the coefficient of thermal expansion of

$$\text{Ti–O RMC: } 1.02 \pm 0.04 \times 10^{-5} \text{ K}^{-1}$$
$$\text{Sr–O RMC: } 1.24 \pm 0.03 \times 10^{-5} \text{ K}^{-1}$$
$$\text{Ti–O and Sr–O Rietveld: } 0.78 \pm 0.02 \times 10^{-5} \text{ K}^{-1}$$

(where the values for the two coefficients in the Rietveld refinements are the same because both are entirely due to the linear thermal expansion of the lattice). The thermal expansion from the RMC data is larger than from the Rietveld analysis in both cases.

The same effect was seen in even more dramatic fashion in our previous work on the phases of silica [25–27]. In these phases, the RMC results show a small thermal expansion of the Si–O bond, consistent between different polymorphs [28], whereas the distances between the mean positions of the Si and O atoms obtained from Rietveld refinement are even seen to
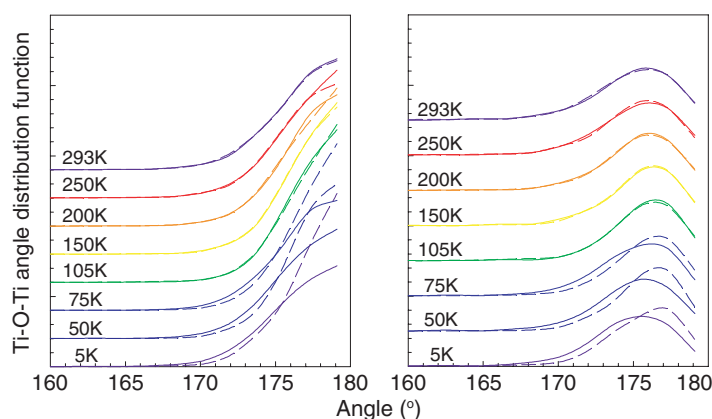
Figure 10. Ti–O–Ti distribution functions $f(\theta)/\sin\theta$ (left) and $f(\theta)$ (right) as described in the text, showing data for bond linkages normal and parallel to the [001] direction as continuous and broken lines respectively.

contract on heating. In the silica phases, this effect is associated with the rotational motions of the SiO_4 tetrahedra, such that the distance between the mean Si and O positions (the quantity obtained from the Rietveld results) is smaller than the instantaneous bond lengths (the result obtained from RMC). In the silica phases, the thermal expansion of the Si–O bond is larger than the expansion of the distance between the mean Si and O positions, the latter being negative for some temperatures. In the case of $SrTiO_3$, the difference between the thermal expansion of the Ti–O distance is probably due to the existence of the rotational motions of the TiO_6 octahedra in an analogous manner, but the effect is somewhat smaller than in silica. It is not clear why there should be the same effect for the Sr–O bond, but it is likely that it is associated with the fact that the predominant thermal motion of the O atoms is at an angle to the Sr–O direction. In fact it is interesting that the thermal expansion of the Sr–O bond is larger than that of the Ti–O bond, and there is a greater difference between the RMC and Rietveld values in this case.

4.2.2. Ti–O–Ti angle distribution functions. Figure 10 shows two representations of the distribution function for the Ti–O–Ti bond angles, θ, namely the pure distribution function $f(\theta)$ and the modified distribution function $f(\theta)/\sin\theta$. The problem with $f(\theta)$ is that in three dimensions the number of angles around any value of θ is proportional to $\sin\theta$, so that it is impossible to obtain a peak around $\theta = 180°$ even if the bond is merely fluctuating around this angle. On the other hand, $f(\theta)$ shows a clearer peak for $\theta \neq 180°$ in the low-temperature phase where the bond angle fluctuations about a non-linear configuration. In both representations in figure 10 we show separately the distribution functions for Ti–O–Ti linkages in the [001] direction and normal to this direction.

The distribution functions clearly show the effect of the phase transition, with the peak in $f(\theta)$ clearly moving away from $\theta = 180°$ on cooling, and a clear change in the shape of $f(\theta)/\sin\theta$ on cooling below the phase transition. The distribution function shows the existence of small fluctuations in the bond angle of around 5° in the high-temperature phase, with small increases on heating. These fluctuations arise from small rotations of the TiO_6 octahedra. The key result from figure 10 is that the fluctuations in the rotations of the TiO_6 octahedra are small even at the highest temperature. The distribution becomes narrower on cooling, and below the phase transition the distribution function splits into the two symmetrically distinct distributions.

4.2.3. TiO_6 orientation distribution function. We have used a method, based on geometric algebra [37] and implemented in the program GASP [38], to compare the TiO_6 octahedra
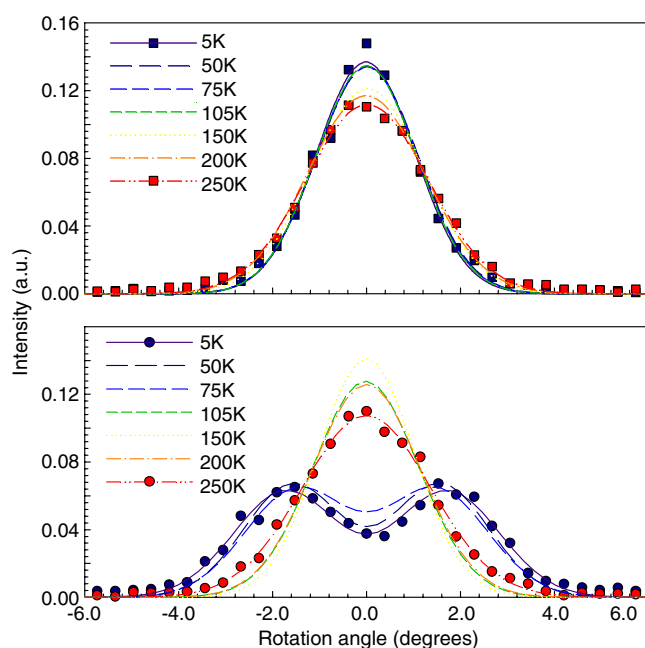
Figure 11. Distribution of TiO$_6$ rotations as described using geometric analysis. Top shows the x, y rotor distributions, and bottom shows the z rotor distributions.

in an RMC-generated structure to those in the average high-symmetry structure. For each polyhedron we obtain a rotor describing its rotation relative to the average orientation. To first order, the z-component of the rotor represents the degree of rotation about the z-axis and so on.

The distribution of the z rotor components, figure 11 has a single peak centred at 0° for $T > 105$ K; however, the z rotor component shows a bimodal distribution at $T < 105$ K, with peaks corresponding to the positive and negative rotations. The mean rotation angle obtained from this analysis is plotted in figure 7 for comparison with the Rietveld refinement results. On the other hand, the distribution of x and y rotor components (which are symmetrically equivalent, and equal to the z-distribution in the high-temperature phase) merely show a single peak for all temperatures which sharpens on cooling.

5. Discussion

5.1. Comparison with quartz

Comparison of the results presented above with a similar study on quartz is instructive [25, 26]. The latter case also has a displacive phase transition involving rotations of polyhedra, in this case SiO$_4$ tetrahedra. The interesting point about this study is that there are significant points of difference between the two systems, as well as some similarities.

The main difference between quartz and SrTiO$_3$ concerns the amplitude of orientational fluctuations of the structural polyhedra in the high-temperature phase, which are much larger in quartz than in SrTiO$_3$. The relatively small amplitudes of fluctuations in the high-temperature phase of SrTiO$_3$ are seen in figures 10 and 11. Consistent with this is the fact that the effect on the distances between the mean-positions of bonded atoms is larger, and more dramatic, in quartz than in SrTiO$_3$. Moreover, the amplitude of rotation that freezes into the structure is only 2° in SrTiO$_3$ and nearly 20° in quartz. This order-of-magnitude difference in the distortion of the structure is reflected in a similar difference in the scale of fluctuations.

A related point is that the high-temperature phase of quartz has much more disorder in terms of the arrangement of the orientations of the structural polyhedra, as seen in the RMC configurations, than $SrTiO_3$, as seen in figure 5. In quartz this disorder arises from orientational fluctuations with many wavevectors. The reason for this difference is traced to a fundamental difference in the vibrational dynamics that is related to the topological freedom of the network of the polyhedra, as will be discussed below.

The main point of similarity between $SrTiO_3$ and quartz is that the polyhedra orientation functions for both systems have a single peak in the high-temperature phases and multiple peaks in the low-temperature phases (two in the case of $SrTiO_3$ and three in the case of quartz). This suggests that the polyhedra are rotating about their mean orientations in the high-temperature phase, rather than hopping between distinct orientations. Thus the phase transition in $SrTiO_3$ from the perspective of the short-range structure is fully consistent with a classical displacive phase transition.

5.2. Geometric algebra analysis of the nature of the atomic dynamics

In the case of quartz, information on the relative importance of rigid-unit and distortive motion was obtained by comparing independent RMC configurations at a given temperature [38]. Each RMC configuration represents a 'snapshot' of the structure. Two or more snapshots at the same temperature can be compared either atom by atom—from which we obtain the RMS displacement of all atoms—or polyhedron by polyhedron. In the latter case, for each polyhedron we obtain both a rotation (for the reorientation of the polyhedron) and a residual distortion. The RMS distortion represents the part of a typical oxygen atom's motion that cannot be accounted for by rigid-body motions of the polyhedra. This can be decomposed into a component due to stretching of the Ti–O bond, and the remainder due to bending of O–Ti–O angles.

Our analysis has shown very little temperature dependence of the partitioning of motions between the three types of motion. Averaging over all temperatures, we obtain the following:

Fraction of motion accounted for by TiO_6 rotations: 0.37 ± 0.01

Fraction of motion accounted for by Ti–O stretch: 0.19 ± 0.01

Fraction of motion accounted for by O–Ti–O bend: 0.44 ± 0.02.

These results are in strong contrast to those for quartz [38]. In quartz the ratio of distortive to total motion for vertex oxygens drops from ∼50% at low temperature to only 15–20% at high temperature, showing the dominance of rotational motions in the high-temperature dynamics, and the bending and stretching components are in a ratio of approximately 4:1. This is consistent with the observation of greater orientational disorder in quartz than in $SrTiO_3$.

5.3. Rigid unit modes in $SrTiO_3$ and quartz

The differences between $SrTiO_3$ and quartz can be understood in terms of the 'Rigid Unit Mode' model [29, 31, 32]. The idea is that there may be a set of phonon modes that will propagate without distortions of the constituent structural polyhedra (SiO_4 tetrahedra or TiO_6 octahedra), which are called the Rigid Unit Modes (RUMs). Quartz and $SrTiO_3$ are both frameworks of corner-linked polyhedra, with phase transitions in which a low-symmetry form is obtained from a higher-symmetry form by the condensation of a soft mode involving rotation of the polyhedra, namely a RUM, at one specific wavevector ($\mathbf{k} = (\frac{1}{2}, \frac{1}{2}, \frac{1}{2})$ in the case of the phase transition in $SrTiO_3$). However, in both cases RUMs can exist with other wavevectors, and it is in this point that the differences between $SrTiO_3$ and quartz outlined above can be rationalized.

The soft mode associated with the phase transition in $SrTiO_3$ can be identified as a RUM since the TiO_6 octahedra simply rotate without inducing any first-order distortions of the octahedra. In fact there is a single RUM for all edges of the cubic Brillouin zone, i.e. for **k** along the lines linking $(\frac{1}{2}, \frac{1}{2}, 0)$ to $(\frac{1}{2}, \frac{1}{2}, \frac{1}{2})$ and the lines of equivalent symmetry. This point, demonstrated in a case study by Giddy *et al* [29], is consistent with inelastic neutron scattering measurements of the phonon dispersion curves [30]. On the other hand, in quartz there are planes of wavevectors in reciprocal space that contain RUMs, rather than the RUMs being restricted to lines of wavevectors as in $SrTiO_3$ [31]. This implies that there should be much more overall RUM flexibility in quartz than in $SrTiO_3$. Our data demonstrate this point very clearly on several counts. *First*, the fluctuations in the rotations of the TiO_6 octahedra, as shown in figures 10 and 11, are very much smaller than the corresponding fluctuations in quartz. *Second*, the RMC + GA analysis has shown that the RUM component of the atomic motion is much smaller in $SrTiO_3$ than in quartz. Thus $SrTiO_3$ displays more restricted dynamics, in which the rotational motions are small, and rotational and distortive motions are equally important, with considerably less orientational disorder in the high-temperature phase.

6. Conclusion

This paper has reported the results of a total scattering study of the phase transition in $SrTiO_3$ and the analysis of the data using the RMC method. This has given a new glimpse at the atomic motions associated with the phase transition from a local perspective. We have shown, in contrast to the case of quartz, that the atomic dynamics are not dominated by the RUM motions, and that the behaviour on a local scale closely follows the long-range order. On the other hand, similar to quartz we find that the octahedral motions in the high-temperature phase do not involve hopping between well-defined orientations but follow the form expected for a classical soft-mode driven displacive phase transition.

Acknowledgments

References

[1] Cowley R A 1996 The phase transition of strontium titanate *Phil. Trans. R. Soc.* A **354** 2799–814
[2] Fleury P A, Scott J F and Worlock J M 1968 Soft phonon modes and the 110 K phase transition in $SrTiO_3$ *Phys. Rev. Lett.* **21** 16–9
[3] Cowley R A, Buyers W L and Dolling G 1969 Relationship of normal modes of vibration of strontium titanate and its antiferroelectric phase transition at 110 K *Solid State Commun.* **7** 181–4
[4] Shirane G and Yamada Y 1969 Lattice dynamical study of the 110 K phase transition in $SrTiO_3$ *Phys. Rev.* **177** 858–69
[5] Bruce A D and Cowley R A 1981 *Structural Phase Transitions* (London: Taylor and Francis)
[6] Hunnefeld H, Niemoller T, Schneider J R, Rutt U, Rodewald S, Fleig J and Shirane G 2002 Influence of defects on the critical behavior at the 105 K structural phase transition of $SrTiO_3$: on the origin of the two length scale critical fluctuations *Phys. Rev.* B **66** 014113
[7] Mishina E D, Misuryaev T V, Sherstyuk N E, Lemanov V V, Morozov A I, Sigov A S and Rasing T 2000 Observation of a near-surface structural phase transition in $SrTiO_3$ by optical second harmonic generation *Phys. Rev. Lett.* **85** 3664–7
[8] Hayward S A and Salje E K H 1999 Cubic–tetragonal phase transition in $SrTiO_3$ revisited: Landau theory and transition mechanism *Phase Transit.* **68** 501–22
[9] Salje E K H, Gallardo M C, Jimenez J, Romero F J and del Cerro J 1998 The cubic–tetragonal phase transition in strontium titanate: excess specific heat measurements and evidence for a near-tricritical, mean field type transition mechanism *J. Phys.: Condens. Matter* **10** 5535–43

[10] Geday M A and Glazer A M 2004 Birefringence of SrTiO$_3$ at the ferroelastic phase transition *J. Phys.: Condens. Matter* **16** 3303–10

[11] Itoh M, Yagi T, Uesu Y, Kleemann W and Blinc R 2004 Phase transition and random-field induced domain wall response in quantum ferroelectrics (SrTiO$_3$)-O-18: review and perspective *Sci. Technol. Adv. Mater.* **5** 417–23

[12] Kleemann W, Dec J, Wang R P and Itoh M 2003 Nonlinear susceptibility and phase transition in (SrTiO$_3$)-^{18}O *Phys. Rev.* B **67** 092107

[13] Grupp D E and Goldman A M 1997 Indications of a $T = 0$ quantum phase transition in SrTiO$_3$ *Phys. Rev. Lett.* **78** 3511–4

[14] Hasebe H, Tsujimi Y, Wang R P, Itoh M and Yagi T 2003 Dynamical mechanism of the ferroelectric phase transition of (SrTiO$_3$)-^{18}O studied by light scattering *Phys. Rev.* B **68** 014109

[15] Gallardo M C, Burriel R, Romero F J, Gutierrez F J and Salje E K H 2002 Low-temperature calorimetric study of SrTiO$_3$ *J. Phys.: Condens. Matter* **14** 1881–6

[16] Kityk A V, Schranz W, Sondergeld P, Havlik D, Salje E K H and Scott J F 2000 Nonlinear elastic behaviour of SrTiO$_3$ crystals in the quantum paraelectric regime *Europhys. Lett.* **50** 41–7

[17] Kiat J M and Roisnel T 1996 Rietveld analysis of strontium titanate in the Müller state *J. Phys.: Condens. Matter* **8** 3471–5

[18] Buckley A, Rivera J P and Salje E K H 1999 Twin structures in tetragonal SrTiO$_3$: the ferroelastic phase transition and the formation of needle domains *J. Appl. Phys.* **86** 1653–6

[19] Koga T, Lu Z, Munakata K, Hatakeyama M, Soejima Y and Okazaki A 1995 Domain population in SrTiO$_3$ below the cubic-to-tetragonal phase transition *Phase Transit.* **54** 109–16

[20] McGreevy R L and Pusztai L 1988 Reverse Monte Carlo simulation: a new technique for the determination of disordered structures *Mol. Simul.* **1** 359–67

[21] McGreevy R L 1995 RMC—Progress, problems and prospects *Nucl. Instrum. Methods* A **354** 1–16

[22] Tucker M G, Dove M T and Keen D A 2001 Application of the reverse Monte Carlo method to crystalline materials *J. Appl. Crystallogr.* **34** 630–8

[23] Dove M T, Tucker M G and Keen D A 2002 Neutron total scattering method: simultaneous determination of long-range and short-range order in disordered materials *Eur. J. Mineral.* **14** 331–48

[24] Williams W G, Ibberson R M, Day P and Enderby J E 1998 GEM—general materials diffractometer at ISIS *Physica* B **241–243** 234–6

[25] Tucker M G, Dove M T and Keen D A 2000 Simultaneous measurements of changes in long-range and short-range structural order at the displacive phase transition in quartz *J. Phys.: Condens. Matter* **12** L723–30

[26] Tucker M G, Keen D A and Dove M T 2001 A detailed structural characterisation of quartz on heating through the $\alpha-\beta$ phase transition *Mineral. Mag.* **65** 489–507

[27] Tucker M G, Squires M D, Dove M T and Keen D A 2001 Dynamic structural disorder in cristobalite: neutron total scattering measurement and reverse Monte Carlo modelling *J. Phys.: Condens. Matter* **13** 403–23

[28] Tucker M G, Dove M T and Keen D A 2000 Direct measurement of the thermal expansion of the SiO bond by neutron total scattering *J. Phys.: Condens. Matter* **12** L425–30

[29] Giddy A P, Dove M T, Pawley G S and Heine V 1993 The determination of rigid unit modes as potential soft modes for displacive phase transitions in framework crystal structures *Acta Crystallogr.* A **49** 697–703

[30] Stirling W G 1972 Neutron inelastic scattering study of the lattice dynamics of strontium titanate *J. Phys. C: Solid State Phys.* **5** 2711–30

[31] Hammonds K D, Dove M T, Giddy A P, Heine V and Winkler B 1996 Rigid unit phonon modes and structural phase transitions in framework silicates *Am. Mineral.* **81** 1057–79

[32] Dove M T 1997 Theory of displacive phase transitions in minerals *Am. Mineral.* **82** 213–44

[33] Wells S A, Dove M T, Tucker M G and Trachenko K O 2002 Real-space rigid unit mode analysis of dynamic disorder in quartz, cristobalite and amorphous silica *J. Phys.: Condens. Matter* **14** 4645–57

[34] Toby B H 2001 EXPGUI, a graphical user interface for GSAS *J. Appl. Crystallogr.* **34** 210–21

[35] Larson A C and von Dreele R B 2000 General structure analysis system (GSAS) *Los Alamos Nat. Lab. Report* LAUR 86-748

[36] Keen D A 2001 A comparison of various commonly used correlation functions for describing total scattering *J. Appl. Crystallogr.* **34** 172–7

[37] Wells S A, Dove M T and Tucker M G 2002 Finding best-fit polyhedral rotations with geometric algebra *J. Phys.: Condens. Matter* **14** 4567–84

[38] Wells S A, Dove M T and Tucker M G 2004 Reverse Monte Carlo with geometric analysis RMC + GA *J. Appl. Crystallogr.* **37** 536–44